Journal of *Marine Science and Engineering*

MDPI

Article

Maritime Broadband Communication: Wireless Channel Measurement and Characteristic Analysis for Offshore Waters

Changzhen Li [1], Junyi Yu [2], Jie Xue [3,*,†], Wei Chen [4,5,*,†], Shoufeng Wang [2] and Kun Yang [6,7]

1 School of Information Engineering, Wuhan University of Technology, Wuhan 430070, China; changzhen.li@whut.edu.cn
2 Samsung Research China—Beijing (SRC-B), Beijing 100028, China; junyisrcb.yu@samsung.com (J.Y.); sf.wang@samsung.com (S.W.)
3 Safety and Security Science Group (S3G), Faculty of Technology, Policy and Management, Delft University of Technology, Delft 2600, The Netherlands
4 School of Automation, Wuhan University of Technology, Wuhan 430070, China
5 National Engineering Research Center for Water Transportation Safety, Wuhan 430063, China
6 School of Information Engineering, Zhejiang Ocean University, Zhoushan 316022, China; yangkun@zjou.edu.cn
7 Super Radio AS, 1208 Oslo, Norway
* Correspondence: j.xue@tudelft.nl (J.X.); greatchen@whut.edu.cn (W.C.)
† These authors contributed equally to this work.

Abstract: For a long time, the development of maritime communication has been restricted by the low data rate, high-latency and high cost of the current communication systems. The upgrade of new generation mobile communication technologies is attracting more and more attention to conduct a shore-based broadband mobile communication network with high-latency and high reliability to serve the maritime industries. This paper presents a solution by means of building a ship-to-infrastructure (S2I) and a ship-to-ship (S2S) wireless communication networks for an offshore region. We characterize the S2I and S2S channels at 5.9 GHz band based on the channel measurements in realistic environments. The channel characteristics, including power delay profile, delay spread, propagation path loss, are extracted and analyzed. In view of the difference between marine and terrestrial communications, we analyze the influencing factors of the offshore water, including effective reflection, divergence and shadowing from the water surface, and diffraction loss caused by the earth curvature. We also predict the power coverage range and the channel capacity for S2I and S2S wireless communications. Finally, the communication performance is evaluated according to the channel measurement and characterization analysis. The research results can be a reference for the construction of maritime communication networks.

Keywords: shore-based maritime communications; channel measurement; maritime safety; performance evaluation

Citation: Li, C.; Yu, J.; Xue, J.; Chen, W.; Wang, S.; Yang, K. Maritime Broadband Communication: Wireless Channel Measurement and Characteristic Analysis for Offshore Waters. *J. Mar. Sci. Eng.* **2021**, *9*, 783. https://doi.org/10.3390/jmse9070783

Academic Editor: Mohamed Benbouzid

Received: 7 July 2021
Accepted: 16 July 2021
Published: 20 July 2021

1. Introduction

To date, the new generation of mobile communication technology represented by 5G has been developing rapidly. It is providing fast and reliable communication services for various industries, such as vehicular communications [1,2], high-speed railway communications [3,4], telemedicine communications [5]. As an essential part of the national economy, marine industry also needs to develop towards intelligence and digitization, relying on the new generation of mobile communication technology. Furthermore, the national Exclusive Economic Zones (EEZ) are generally constructed in the coastal water region where undertake a lot of important national tasks and maritime activities, e.g., inshore cultivating and fisheries, oil and gas exploration and production. Therefore, a high-speed and reliable data transmission system should be built to guarantee the smooth contact between vessels and control center. Especially, with the development of offshore in-

dustry and smart ocean, and the ever-growing maritime economy, a more reliable wireless communication system with a higher data rate and a low cost is required urgently for the frequent maritime activities.

Conventional communication systems used in offshore waters mainly include maritime radio communication, maritime satellite communication, and shore-based mobile communication based on terrestrial cellular networks. The maritime radio communication systems are customarily operated in MF/HF/VHF bands with a short coverage and a low data rate [6–8]. The satellite communication system can provide wide data coverage for the global areas, while the large propagation delay and high implementation cost limit the usage in maritime communications [9,10].

Compared to the above two communication systems, the development of the shore-based mobile communication system for offshore waters is lagging behind. However, the current maritime wireless communication systems are difficult to meet the demand for smart ocean construction. It is thus attracting more and more interest to build a network on the basis of terrestrial communications for the offshore waters, such as 4G-LTE and 5G [11,12] communication technologies.

In addition, the guarantee of maritime safety also depends on fluent wireless communication technology to some extent. In coastal areas, most ships transmit and receive data via wireless communications networks based on radio frequency (RF), long-term evolution (LTE). Based on the ship-to-ship and ship-to-shore communication technologies, ships can be monitored and controlled remotely and the vessel status information to prevent ship-related accidents can be shared with each other [13]. With the development of wireless communication technology, millimeter wave (mm-Wave) is used to construct the collision prevention system as well, which is expected to replace the automatic identification system with a low data transmission [14].

Furthermore, the construction of smart ocean, including Internet of Ships (IoS), maritime data management and analysis, safety and security considerations, smart ships, smart transportation, smart ports, all depend on a fast and reliable wireless communication network [15].

The fifth-generation mobile communication technology (5G) has provided new solutions of maritime shore-based communication [16,17], such as the world's first maritime 5G communication project titled "LTE, Wi-Fi and 5G Massive MIMO Communications in Maritime Propagation Environments (MAMIME)", which aims to develop the optimized LTE and Wi-Fi systems, and to research the dedicated 5G solutions for the maritime applications [18,19]. Through exploration and research, it is found that the propagation of wireless signals over the water is different from the terrestrial communications. From the perspective of the wireless propagation environments, the offshore wireless channel characteristics will be affected by the mixed factors of land and water. For the open propagation environment of the deep sea region, the reflection and shadowing of the sea surface will make an impact on the wireless channel. Moreover, the earth curvature should also be considered as an important influencing factor in long-distance wireless communication.

Therefore, considering the difference between water communication and terrestrial communication and the perspective of wireless broadband network deployment and optimization, it is necessary to extract typical channel characteristics through actual channel measurement and build a channel model for the research of offshore wireless communication. This paper presents the ship-to-infrastructure and ship-to-ship wireless channel measurements over the offshore water at 5.9 GHz band with a bandwidth of 100 MHz. Additionally, channel measurements description, typical measurement results and channel characteristics are summarized and presented. The contributions of this paper can be summarized as follows:

- The broadband wireless channel measurements over the offshore water are presented. In the measurements, 5.9 GHz and 100 MHz are employed as the carrier frequency and bandwidth, respectively. The temporary S2I and S2S wireless communication networks are built.

- Typical wireless channel characteristics over the offshore water are extracted. Based on the measurement data, the channel characteristics, including power delay profile, delay spread and propagation path loss are analyzed. The impact from water surface on the wireless channel characteristics are presented.
- According to the parameter of the measurement campaign and environment, the effective coverage range of the wireless signal and the channel capacity over the offshore water are predicted and the communication performance is evaluated.

The remainder of this paper is organized as follows. In Section 2, the S2I and S2S wireless channel measurements over the offshore water are presented. The measurement data pre-processing and the analysis method are provided. The typical wireless channel characteristics over the offshore water, including power delay profile, delay spread, propagation path loss, and the impact from the water surface, are extracted and analyzed in Section 3. Performance evaluation of offshore communications is predicted by the effective coverage and channel capacity calculating in Section 4. Finally, conclusions are drawn in Section 5.

2. Experiments

In the present paper, we designed and built a ship-to-infrastructure (S2I) and a ship-to-ship (S2S) temporary mobile communication networks on the Jiaozhou Bay, China, to carry out the wireless channel measurement experiments.

2.1. Ship-to-Infrastructure Wireless Channel Measurement

The temporary S2I mobile communication network was built on the basis of a high-precision signal generation system, including a time-division multiplexing single-input single-output (SISO) channel sounder provided by Super Radio AS in Norway and Norwegian University of Science and Technology (NTNU) [20], transmitter (Tx) and receiver (Rx) antennas, and high-resolution global positioning system (GPS) receivers. The S2I wireless channel measurement had been conducted at 5.9 GHz band with a bandwidth of 100 MHz and a transmit power of 16 dBm. Chirp signal with 10 ns delay resolution was emitted from transmitter part. The receiver part would receive 1933 chirp signals in 1 s. An omni-directional antenna with the gain of 10 dBi and a directional antenna with 16 dBi gain and 3 dB beam-width of 90° (H-plane) and 8° (E-plane) were used as Rx and Tx antennas, respectively. The heights of the Tx and Rx antennas were 3.13 m and 3.12 m above the water surface. Figure 1 presents the diagrams of the S2I and S2S measurement campaigns.

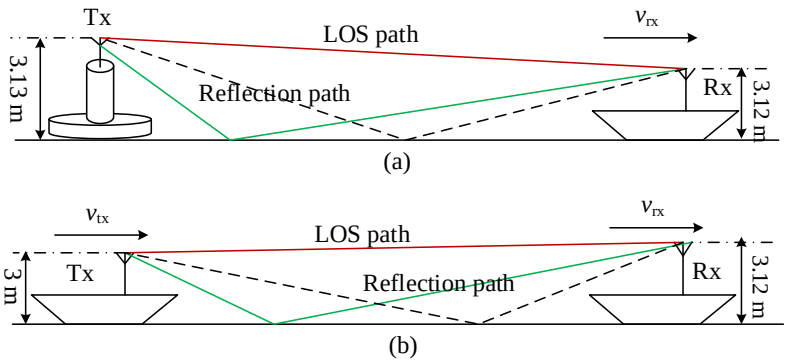

Figure 1. Diagrams of the S2I and S2S measurement campaigns. (**a**) is for S2I and (**b**) is for S2S.

During the measurement, the Tx boat anchored on the pontoon over the sea and another boat carrying the Rx part sailed away from the pontoon with an average speed of 8.37 knots (about 15.5 km/h) in the Jiaozhou Bay. The maximum distance between Tx and Rx parts was 1.35 nautical miles (about 2.5 km).

2.2. Ship-to-Ship Wireless Channel Measurement

The S2S wireless channel measurement was conducted using the same channel sounder and boats in the S2I measurement. Both the Tx and Rx antennas in the S2S measurement were omni-directional antennas with antenna gains of 2 dBi and 10 dBi, respectively. The installation height of the Tx antenna was 3 m, while it was 3.12 m for the Rx antenna.

In the S2S measurement, the Tx and Rx boats sailed in the same direction. The sailing speed of the Tx was between 0.06 knots (0.108 km/h) and 13.2 knots (24.44 km/h), and the speed of the Rx was between 0.66 knots (1.224 km/h) and 11.47 knots (21.24 km/h). The maximum distance between Tx and Rx boats was 0.09 nautical mile (about 168.1 m).

In order to give a more intuitive description, we list the system and measurement parameters in Table reftab:para of the S2I and S2S measurement campaigns.

Table 1. Parameters of Measurement Campaigns.

Parameter	S2I	S2S
Center frequency [GHz]	5.9	5.9
Bandwidth [MHz]	100	100
Delay resolution [ns]	10	10
Tx power [dBm]	16	16
Tx gain [dBi]	16	2
Rx gain [dBi]	10	10
Tx height [m]	3.13	3
Rx height [m]	3.12	3.12

In addition, the measurements are recorded by video as well. Our channel measurements in this paper serve the data collection of a broadband wireless communication channel over the offshore water regions, based on which the typical channel characteristics extraction and analysis of marine wireless channels will be carried out.

2.3. Data Pre-Processing

As mentioned above, the measurement data is collected by the Rx part of the channel sounder. It is saved as the format of the time-variant channel transfer functions (CTF) $H(f,t)$. According to the principle of the channel sounder [21,22], the format of the measurement data can be expressed as a matrix of $m \times n$, where m = 1933 is the total number of chirp signals per second, denoting the time index and n = 2560 is the number of samples in each chirp, representing the delay index. We can then obtain the discretized channel impulse response (CIR) $h(t,\tau)$ by computing the inverse discrete Fourier transform (IDFT) of CTF with respect to the Doppler frequency.

Based on the classical assumption of wide-sense stationary uncorrelated scattering (WSSUS) [23], we should ensure that the radio channel satisfies the WSSUS assumption by setting windows along the measurement time t in the time-variant channel analysis. According to previous related research [24,25], the channel within a few tens of wavelengths can be regarded as a quasi-stationarity channel. Therefore, we adopt 20λ to be the non-overlap window in order to make the channel analysis.

3. Results and Discussion

Based on the S2I and S2S measurements above, we analyze the measurement data to understand the characteristics of the wireless propagation over the sea deeply. Note that, in this paper, we mainly focus on the key characteristics, including power delay profile, delay spread and propagation path loss, which are essential for the research of maritime wireless channels.

3.1. Power Delay Profile

The time-varying instantaneous power delay profiles (PDPs) can characterize the impact of time variations on the received signal power. It shows the relevance of time, delay and received power. According to the wireless communication theories [26], the instantaneous PDPs can be obtained by the square of the time-varying channel impulse response $h(t, \tau)$, shown in Equation (1).

$$P(t, \tau) = \sum_{t} |h(t, \tau)|^2 \tag{1}$$

where $P(t, \tau)$ represents the time-varying instantaneous power delay profiles and $h(t, \tau)$ is the channel impulse response.

Then, the average PDP can be obtained by the average operator.

$$P_a(\tau) = E\{P(t, \tau)\} \tag{2}$$

where P_a represents the average power delay profile, τ is the delay, P is the power delay profile and E is the average operator.

We obtained the instantaneous PDPs of the S2I and S2S measurements after the data pre-processing, shown in Figure 2a,b. We can find that, for the wireless channel over the sea, the received power decreases with the increase of distance. Since the measurement has been conducted over the sea, which is an open propagation environment, the wireless signal transmits mainly through the line-of-sight (LOS) path compared with the terrestrial communications, such as vehicular communication [27] and high-speed railway communication [24,25,28]. Furthermore, we note that the reflection path and other characteristics that need attention appear in some specific areas as well. In the S2I and S2S measurements, areas I–III and i–iii are marked in the PDP results, as shown in Figure 2. Areas I, i and iii are selected due to the strong received power with the short communication distance, while areas II, III and ii are with reflection paths caused by the surroundings or other factors.

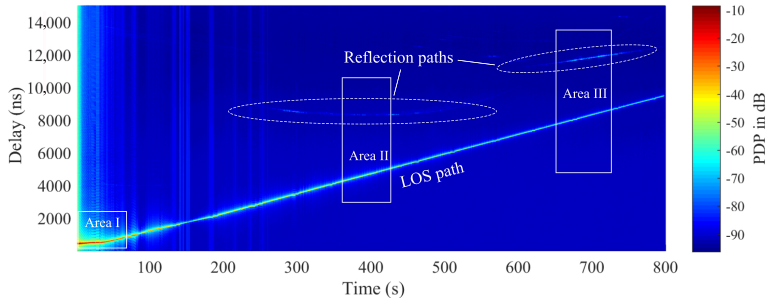

(**a**)

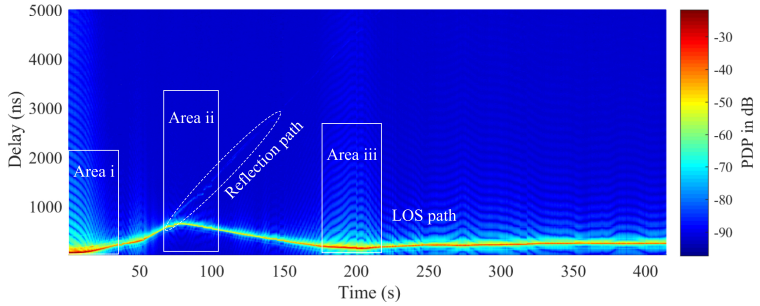

(**b**)

Figure 2. Power delay profiles for the two measurements. (**a**) is for S2I and (**b**) is for S2S.

To analyze the wireless channel characteristic from the view of the received power and multi-path effect. The average PDPs are extracted from the selected areas I–III for S2I and areas i–iii for S2S measurements, shown in Figure 3. We choose the data within 1 sec to calculate the average PDP from the selected areas, respectively. In the S2I measurement, the Rx gradually moved away from the boat that docked at the pontoon. We can find that the delay of the LOS path is increasing with a decreasing received power, where the average power received by the LOS component is −20.81 dB, −46.49 dB, −56.65 dB for cases I, II, III, respectively, as shown in Table 2. From the results of the average PDP, it can also be noted that the noise is more obvious when the distance between Rx and Tx is small. The shaking of the measurement boat may cause this due to the wave.

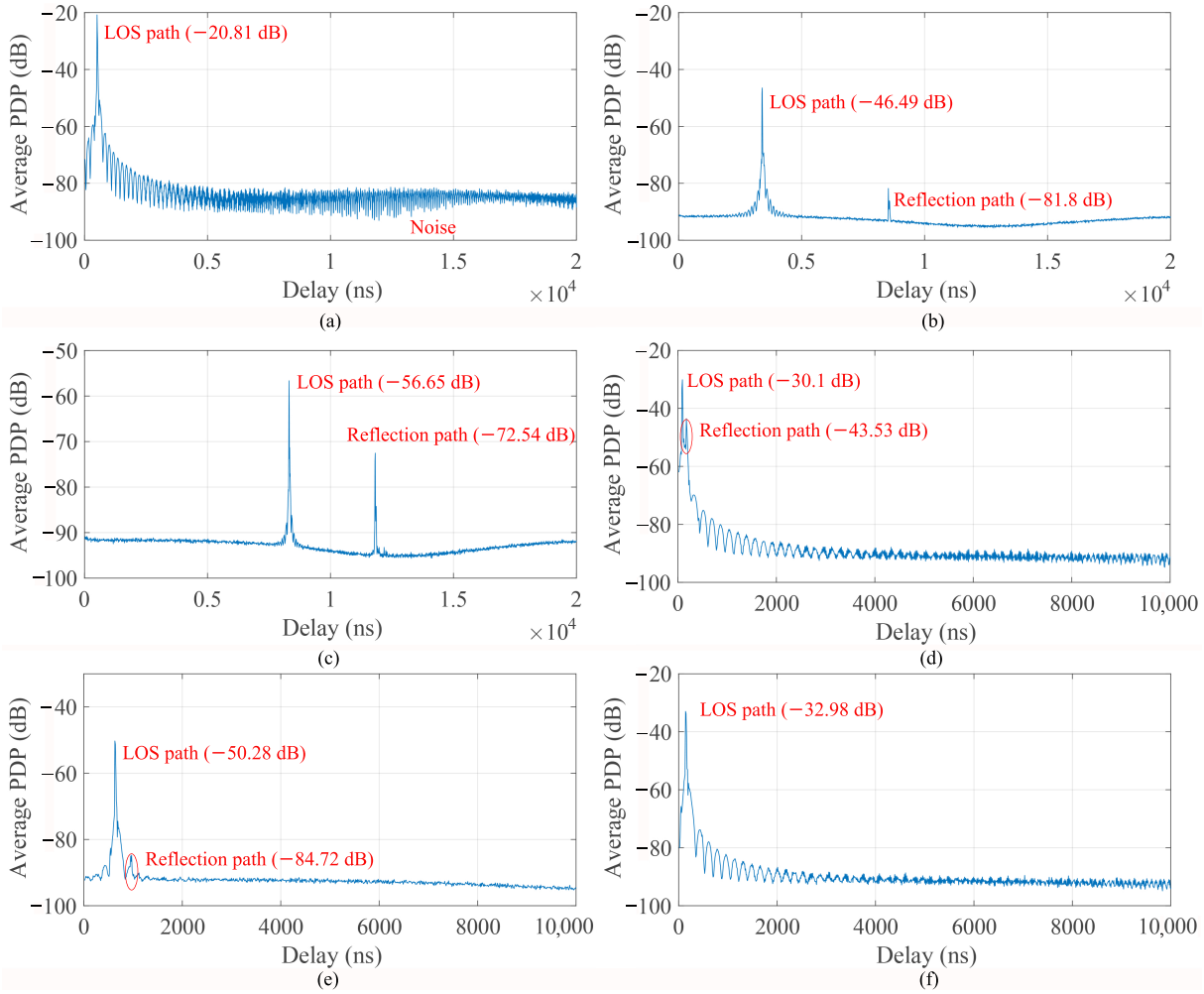

Figure 3. Average PDP from the three selected areas. (**a**–**c**) are Area I–III in S2I measurement, (**d**–**f**) are Area i–iii in S2S measurement.

Table 2. Results of the average PDP.

Area	Parameter	I	II	III	i	ii	iii
LOS	Delay (ns)	510	3400	8320	90	630	140
LOS	Avreage power (dB)	−20.81	−46.49	−56.65	−30.1	−50.28	−32.98
NLOS	Delay (ns)	-	8530	1.182×10^4	170	970	-
NLOS	Avreage power (dB)	-	−81.8	−72.54	−43.53	−84.72	-

3.2. RMS Delay Spread

Delay spread is one of the key parameters for wireless communication. Based on the measurement data, we can obtain the root mean square (RMS) delay spread shown in

Equation (3) by the second-order central moment of the power delay profile, after the noise removal using a threshold of 6 dB above the average noise floor [29,30].

$$\tau_{rms} = \sqrt{\frac{\int_{-\infty}^{\infty} P_a(\tau)\tau^2 d\tau}{\int_{-\infty}^{\infty} P_a(\tau) d\tau} - \left(\frac{\int_{-\infty}^{\infty} P_a(\tau)\tau d\tau}{\int_{-\infty}^{\infty} P_a(\tau) d\tau}\right)^2} \tag{3}$$

Corresponding to the measurement time and the result of the power delay profiles, Figure 4 plots the time-variant RMS delay spread. We find that the multi-path components can also make impact on the RMS delay spread, which have been shown in areas II and III of S2I measurement and area ii of S2S measurement. The effect from the short distance can also be found in area I of S2I measurement and areas i and iii of S2S measurement. It is noted that both the multi-path components and the shaking of the boat due to the wave can increase the RMS delay spread.

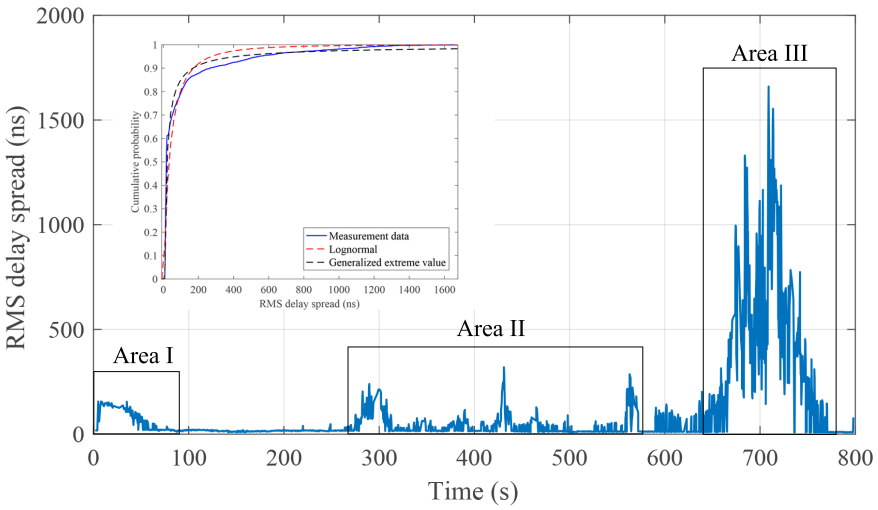

(**a**)

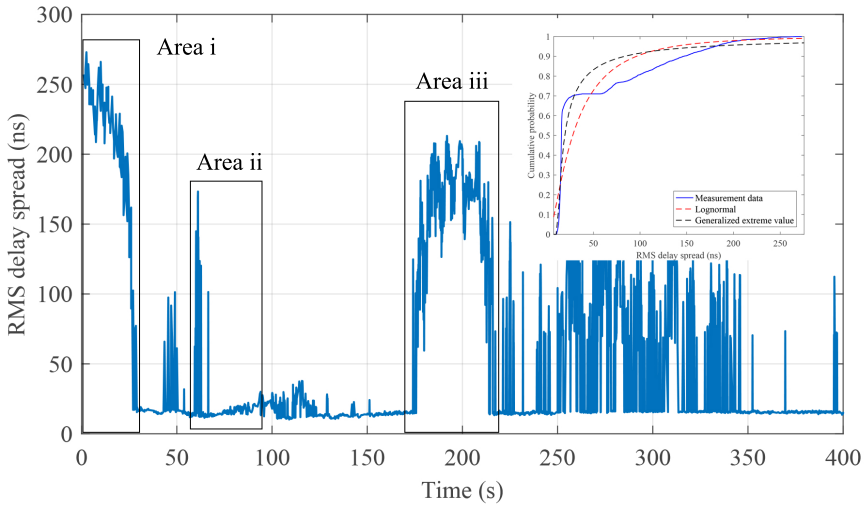

(**b**)

Figure 4. RMS delay spread and the statistical result of the measurements. (**a**) is for S2I and (**b**) is for S2S.

A statistical analysis of the RMS delay spread is also made through the cumulative distribution function (CDF), as shown in Figure 4. The measured RMS delay spreads

are fitted by Lognormal and Generalized Extreme Value distributions, respectively. The result shows that the Lognormal distribution can characterize our measurement data well. Meanwhile, due to the effect of multi-path components and the shaking of the boat, the measurement data also follows the Generalized Extreme Value distribution well. Moreover, Table 3 lists the statistical result obtained from the CDF. It can be found that 50% of the RMS delay spreads for both the measurements are within 17.5 ns, and 75% of those are within 75 ns without an obvious difference. However, 90% of the RMS delay spreads for the S2I measurement is within 265.8 ns, while 146.1 ns for the S2S measurement. This is because the measurement distance of the S2I case is much longer than the S2S case.

Table 3. Statistical result of the RMS delay spread.

Measurement	RMS Delay Spread (ns)		
	50%	75%	90%
S2I	17.52	75.2	265.8
S2S	15.9	70.76	146.1

3.3. Propagation Path Loss

Propagation path loss is caused by the radiation diffusion of transmitting power and the propagation characteristics of a wireless channel, which reflects the change of the average power of a received signal in the macro range. It can be used to characterize the logarithmic relation between the power reduction and the Tx-Rx distance. In the analysis of wireless channel, some channel models have been built, such as free space model, Okumura-Hata model. Based on the actual propagation environment of the sea, Kun et al. [31,32] proposed a quasi-deterministic path loss propagation model for the open sea environment, which have considered the reflection from the water surface, divergence, and earth curvature effect and built a round earth loss model for the wireless channel over the sea.

In this paper, we also use the round earth loss (REL) model to analyze the path loss based on the measurement data. Figure 5 plots the relationship between main influencing factors and Tx-Rx distance. It can be found that the effective reflection coefficient from the water surface increases with the increase of distance, while the divergence coefficient, shadowing coefficient, and diffraction loss caused by earth curvature decrease. The shadowing coefficient is also affected by the different surface slopes, where a larger slope results in a smaller shadowing coefficient at the same Tx-Rx distance. The diffraction loss caused by earth curvature appears beyond the 0.6 First Fresnel Zone D_{06} = 1.94 km, as shown in Figure 5. In addition, the divergence coefficient and the shadowing coefficient will decay to zeros due to the totally shadowed of the reflected rays. The distance for the totally shadowed is 12.63 km for h_{tx} = 3.13 m and h_{rx} = 3.12 m in this paper. However, our measurement distance is within this critical distance; the divergence coefficient and the shadowing coefficient are not reached 0 in this paper. As well, due to our short measurement distance, we obtain a small diffraction loss caused by earth curvature, shown in Figure 5.

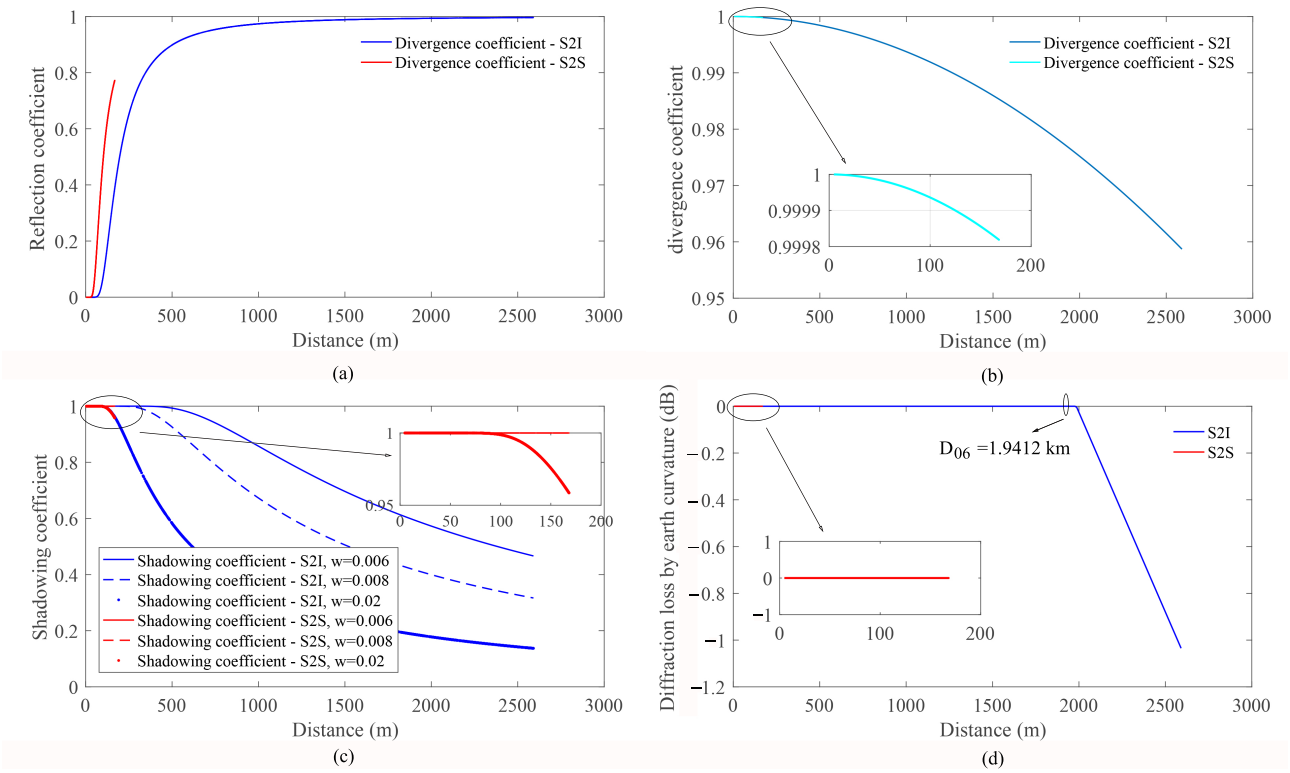

Figure 5. Effect factors. (**a**) effective reflection coefficient from water surface, (**b**) divergence coefficient, (**c**) shadowing coefficient, and (**d**) diffraction loss caused by earth curvature.

By including the factors mentioned above in the two-ray geometrical model [33], the REL model shown in Equation (4) can characterize the propagation path loss comprehensively.

$$PL(d) = 20 \cdot \log_{10}\left(\frac{\lambda}{4\pi D_{\text{los}}}\right) + 20 \cdot \log_{10}(\eta) + L_{\text{diff(e)}} \tag{4}$$

where $\eta = \left|1 + S_{\text{c}} \cdot Div_{\text{eff}} \cdot R_{\text{rough}} \cdot e^{j(2\pi/\lambda)D_{\text{diff}}}\right|$. S_{c}, Div_{eff}, R_{rough}, D_{diff}, $L_{\text{diff(e)}}$ are shadowing coefficient, divergence coefficient, effective reflection coefficient, the phase difference between reflected wave and line of sight (LOS) wave and the diffraction loss derived from earth curvature effect, respectively.

Figure 6 plots the measurement path loss and the fitted results from typical models, including the free space model, one-slope model, ITU-R P.1411 model and REL model. It can be found that the measurement propagation path loss follows the REL model better than other classical models. Moreover, based on the REL model, the comparison result shows that the reflection effect is more obvious on the long-distance S2I measurement than that on the short-distance S2S measurement.

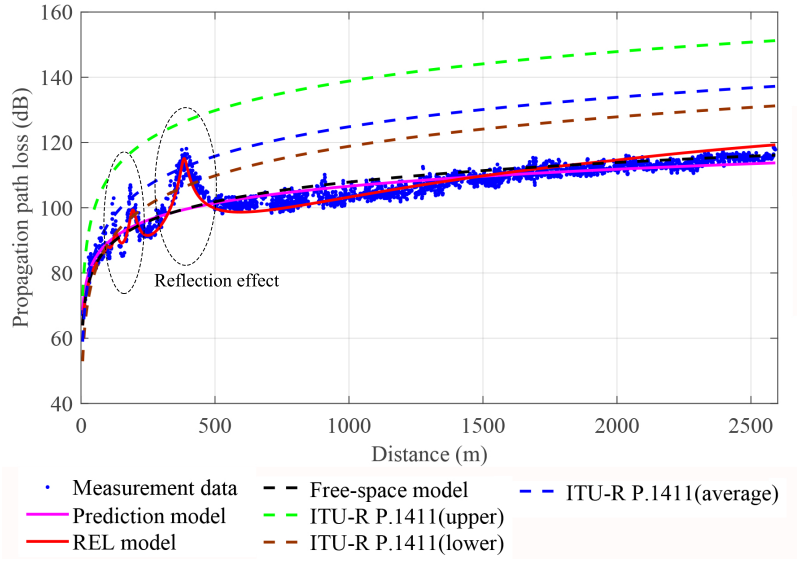

(**a**)

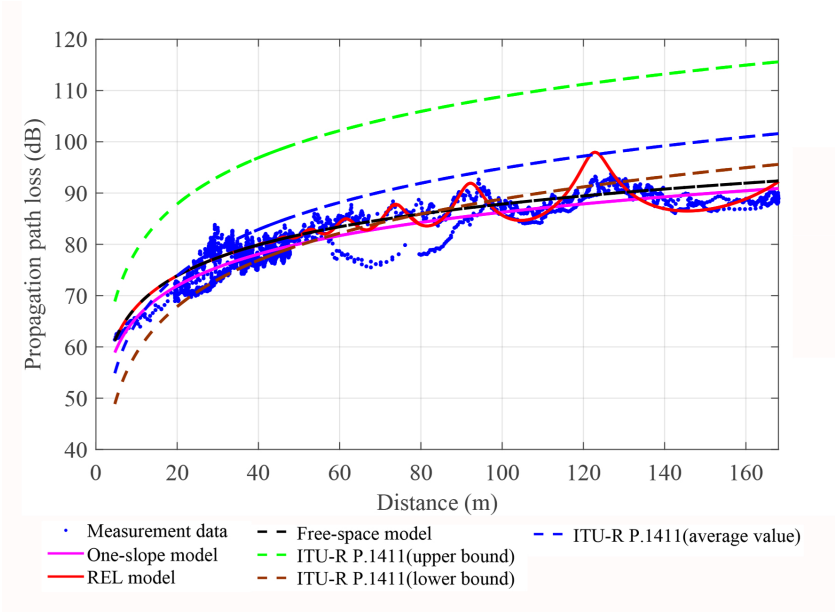

(**b**)

Figure 6. Propagation path loss. (**a**) S2I measurement, (**b**) S2S measurement.

4. Performance Evaluation of Offshore Communications

In order to provide some effective reference to the construction of offshore wireless communication networks, this paper will also make a performance evaluation of the communication capability based on the measurements mentioned above.

4.1. Power Coverage

Based on the measurement channel impulse response (CIR), the received power can be obtained by calculating the square value of the amplitude of the CIR. It represents the real signal level received by the receiver after the transmission of the surrounding environment under the set parameters, including the gain of antennas, the height of the base station and the power of the transmitting equipment. It can contribute to predicting the effective coverage range, which is important to the wireless network planning and base station deployment.

Figure 7 gives the power coverage range based on the S2I measurement. It shows that the received power varies from −92.3 dB to −41.3 dB with the measurement distance. The minimum received power is about −92.3 dB at the Tx-Rx distance of 2500 m, which can still support smooth communication.

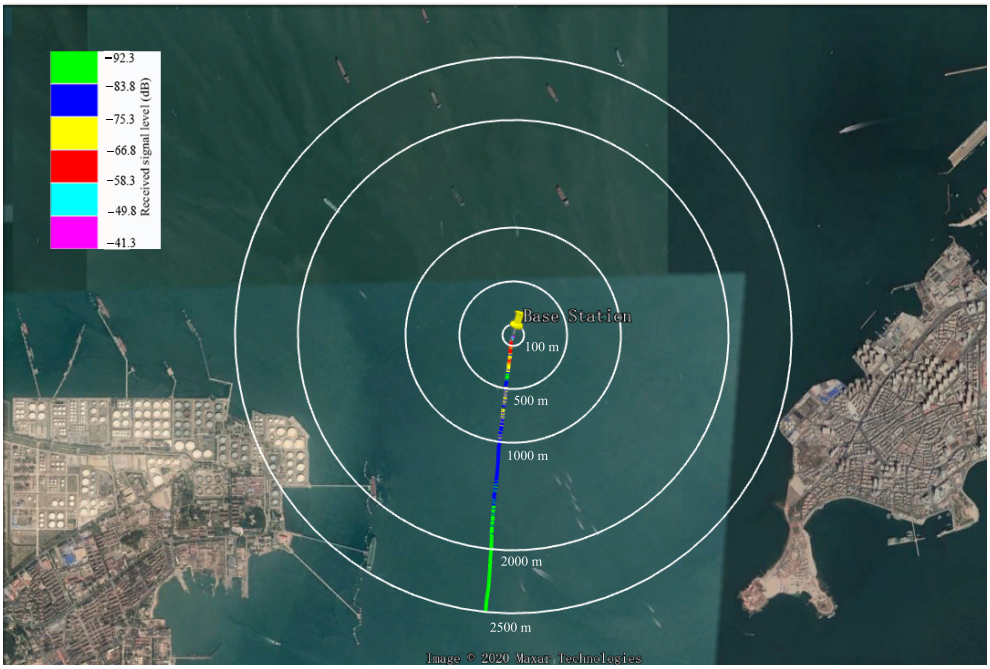

Figure 7. The measured coverage range of S2I communication.

4.2. Channel Capacity

Channel capacity is the minimum upper bound of the achievable rate when information can be reliably transmitted in a channel. According to the description of the Shannon-Hartley theorem [34], the relationship of channel capacity, signal-to-noise ratio and bandwidth of a wireless channel can be summarized by the Equation (5).

$$C = B_w \cdot \log_2\left(1 + 10^{snr/10}\right) \tag{5}$$

where C represents the capacity of the channel on bit per second (b/s), B_w is the bandwidth on Hz and snr is the signal-to-noise ratio on dB.

Based on the collected measurement data, we obtained the channel capacity of the two scenarios. The result indicates that the channel capacity of the S2I and the S2S measurement is 0.47–2.51 Gb/s with an average value of 1.17 Gb/s and 1.21–2.35 Gb/s with an average value of 1.72 Gb/s, as shown in Table 4. The average channel capacity of S2S measurement is bigger than that of S2I measurement due to the short Tx-Rx distance. This average channel capacity is big enough to meet the demand of intelligent shipping communication and support the general data transmission, such as video, monitoring, etc.

Table 4. Results of the channe capacity.

Case	Channel Capacity (Gb/s)	Average Value (Gb/s)
S2I	0.47–2.51	1.17
S2S	1.21–2.35	1.72

According to our description above, the factors that affect the distribution of power, delay spread, and propagation path loss have been analyzed. We find that the main influencing factor for the sea propagation environment is the reflection from the water surface.

Meanwhile, the earth curvature effect is also not neglected for long-distance communication. Therefore, in the planning of the offshore wireless communication network, we should select an appropriate carrier frequency and bandwidth. In addition, the reflection effect from the water surface, the influence of ship motion on energy distribution, the multi-path effect and shadowing from the passing huge ships and buildings on the shore should also be considered.

5. Conclusions

This paper presents the ship-to-infrastructure and ship-to-ship wireless channel measurements over the coastal waters. Based on the measurement data, the channel characteristics, including power delay profile, root means square delay spread, and propagation path loss, are extracted and analyzed. The results demonstrate that the main influencing factor on the root means square delay spread is the distance between Tx and Rx parts for the wireless channel over the sea without other obstacles. Additionally, for the propagation path loss, effective reflection, divergence and shadowing from water surface are the critical influencing factors. Meanwhile, the diffraction loss caused by earth curvature should also not be neglected for the long-distance wireless communication over the sea. Based on the measurement data, we also make a preliminary analysis on the effective power coverage and the channel capacity. The predicting outcomes show that the channel has a good performance with an average channel capacity of 1.17 Gb/s when the Tx-Rx distance is within 2500 m. Our research result can give a reference for the construction of the offshore 5G mobile communication network. However, the channel measurements in this paper only support single-input single-output (SISO) due to the limitation of the channel measurement equipment. In the future, we plan to explore the application of massive MIMO technology to maritime wireless communications.

Author Contributions: C.L.: Methodology, Software, Validation, Formal analysis, Writing—original draft. J.Y.: Measurment, Writing—review & editing. J.X.: Resources, Conceptualization, Funding acquisition, Writing—review & editing. W.C.: Resources, Conceptualization, Funding acquisition, Writing—review & editing. S.W.: Writing—review & editing. K.Y.: Funding acquisition, Equipment. All authors have read and agreed to the published version of the manuscript.

Funding: This document is the results of the research project funded in part by the MAMIME project (no. 256309) by the Norwegian Research Council, in part by the National Natural Science Foundation of China (no. 61701356), in part by the Fundamental Research Funds for the Central Universities (no. 40120638), and in part by the China Scholarship Council (no. 201706950088).

Institutional Review Board Statement: Not applicable.

Informed Consent Statement: Not applicable.

Data Availability Statement: The datasets generated and analyzed during this study are available from the corresponding author upon request.

Acknowledgments: We thank Wuhan University of Technology for their support.

Conflicts of Interest: The authors declare no conflict of interest. The funders had no role in the design of the study; in the collection, analyses, or interpretation of data; in the writing of the manuscript, or in the decision to publish the results.

References

1. Shah, S.A.A.; Ahmed, E.; Imran, M.; Zeadally, S. 5G for vehicular communications. *IEEE Commun. Mag.* **2018**, *56*, 111–117. [CrossRef]
2. Shen, X.; Fantacci, R.; Chen, S. Internet of Vehicles. *Proc. IEEE* **2020**, *108*, 242–245. [CrossRef]
3. Liu, Y.; Wang, C.X.; Huang, J. Recent developments and future challenges in channel measurements and models for 5G and beyond high-speed train communication systems. *IEEE Commun. Mag.* **2019**, *57*, 50–56. [CrossRef]
4. Ai, B.; Molisch, A.F.; Rupp, M.; Zhong, Z.D. 5G Key Technologies for Smart Railways. *Proc. IEEE* **2020**, *108*, 856–893. [CrossRef]
5. Fei, J.; Wang, X.; Wang, W. Application of 5G communication technology in telemedicine. *Inf. Commun. Technol. Policy* **2019**, *45*, 92.

6. Bauk, S. A Review of NAVDAT and VDES as Upgrades of Maritime Communication Systems. In *Advances in Marine Navigation and Safety of Sea Transportation*; CRC Press: Boca Raton, FL, USA, 2019; pp. 81–87.
7. Manoufali, M.; Alshaer, H.; Kong, P.Y.; Jimaa, S. An overview of maritime wireless mesh communication technologies and protocols. *Int. J. Bus. Data Commun. Netw. (IJBDCN)* **2014**, *10*, 1–29. [CrossRef]
8. Valčić, S.; Mrak, Z.; Gulić, M. Analysis of advantages and disadvantages of existing maritime communication systems for data exchange. *Pomorstvo* **2016**, *30*, 28–37. [CrossRef]
9. Ilčev, S.D. *Global Mobile Satellite Communications Theory*; Springer: Berlin, Germany, 2017.
10. Disant, A.; Dias, F. Microwave Propagation in Maritime Environments. *Mar. Technol. Soc. J.* **2020**, *54*, 17–24. [CrossRef]
11. Huo, Y.; Dong, X.; Beatty, S. Cellular Communications in Ocean Waves for Maritime Internet of Things. *IEEE Internet Things J.* **2020**, *7*, 9965–9979. [CrossRef]
12. Li, X.; Feng, W.; Wang, J.; Chen, Y.; Ge, N.; Wang, C.X. Enabling 5G on the Ocean: A Hybrid Satellite-UAV-Terrestrial Network Solution. *arXiv* **2020**, arXiv:2006.00826.
13. Yang, H. A Cost-Effective Ship Safety Data Transfer in Coastal Areas. *J. Coast. Res.* **2018**, 1206–1210. [CrossRef]
14. Lee, M.K.; Park, Y.S. Collision prevention algorithm for fishing vessels using mmWAVE communication. *J. Mar. Sci. Eng.* **2020**, *8*, 115. [CrossRef]
15. Aslam, S.; Michaelides, M.P.; Herodotou, H. Internet of ships: A survey on architectures, emerging applications, and challenges. *IEEE Internet Things J.* **2020**, *7*, 9714–9727. [CrossRef]
16. Mashino, J.; Tateishi, K.; Muraoka, K.; Kurita, D.; Suyama, S.; Kishiyama, Y. Maritime 5G experiment in windsurfing world cup by using 28 GHz band Massive MIMO. In Proceedings of the 2018 IEEE 29th Annual International Symposium on Personal, Indoor and Mobile Radio Communications (PIMRC), Bologna, Italy, 9–12 September 2018; pp. 1134–1135.
17. Zeng, J.; Sun, J.; Wu, B.; Su, X. Mobile edge communications, computing, and caching (MEC3) technology in the maritime communication network. *China Commun.* **2020**, *17*, 223–234. [CrossRef]
18. Norway, S.I. Maritime 5G Will Hasten IoT Adoption in Shipping Industry. 2019. Available online: https://www.hellenicshippingnews.com/maritime-5g-will-hasten-iot-adoption-in-shipping-industry/ (accessed on 25 November 2019).
19. News, H.S. Contributes to the Construction of the World's First Autonomous Ship. 2019. Available online: https://www.smartinnovationnorway.com/nyheter/utvikler-5g-teknologi-som-lar-bater-snakke-med-hverandre/ (accessed on 22 February 2019).
20. Firoozi, F.; Borhani, A.; Pätzold, M. Experimental characterization of mobile fading channels aiming the design of non-wearable fall detection radio systems at 5.9 GHz. In Proceedings of the 2016 IEEE International Conference on Communication Systems (ICCS), Shenzhen, China, 14–16 December 2016; pp. 1–6.
21. Li, C.; Yang, K.; Yu, J.; Li, F.; Shui, Y.; Chang, F.; Chen, W. V2V Radio Channel Performance Based on Measurements in Ramp Scenarios at 5.9 GHz. *IEEE Access* **2018**, *6*, 7503–7514. [CrossRef]
22. Li, C.; Yu, J.; Chen, W.; Wang, K.; Yang, K. Measurements and analysis of vehicular radio channels in the inland lake bridge area. *IET Microw. Antennas Propag.* **2019**, *13*, 1394–1401. [CrossRef]
23. Pätzold, M. *Mobile Radio Channels*; John Wiley & Sons: New York, NY, USA, 2011.
24. Guan, K.; Zhong, Z.; Ai, B.; Kürner, T. Propagation measurements and analysis for train stations of high-speed railway at 930 MHz. *IEEE Trans. Veh. Technol.* **2014**, *63*, 3499–3516. [CrossRef]
25. He, R.; Zhong, Z.; Ai, B.; Wang, G.; Ding, J.; Molisch, A.F. Measurements and analysis of propagation channels in high-speed railway viaducts. *IEEE Trans. Wirel. Commun.* **2012**, *12*, 794–805. [CrossRef]
26. Molisch, A.F. *Wireless Communications*; John Wiley & Sons: New York, NY, USA, 2012; Volume 34.
27. He, R.; Molisch, A.F.; Tufvesson, F.; Zhong, Z.; Ai, B.; Zhang, T. Vehicle-to-vehicle propagation models with large vehicle obstructions. *IEEE Trans. Intell. Transp. Syst.* **2014**, *15*, 2237–2248. [CrossRef]
28. He, R.; Zhong, Z.; Ai, B.; Ding, J.; Yang, Y.; Molisch, A.F. Short-term fading behavior in high-speed railway cutting scenario: Measurements, analysis, and statistical models. *IEEE Trans. Antennas Propag.* **2012**, *61*, 2209–2222. [CrossRef]
29. Abbas, T.; Bernadó, L.; Thiel, A.; Mecklenbrauker, C.F.; Tufvesson, F. Measurements based channel characterization for vehicle-to-vehicle communications at merging lanes on highway. In Proceedings of the 2013 IEEE 5th International Symposium on Wireless Vehicular Communications (WiVeC), Dresden, Germany, 2–3 June 2013; pp. 1–5.
30. Fang, C.; Allen, B.; Liu, E.; Karadimas, P.; Zhang, J.; Glazunov, A.A.; Tufvesson, F. Indoor-indoor and indoor-outdoor propagation trial results at 2.6 GHz. In Proceedings of the 2012 Loughborough Antennas & Propagation Conference (LAPC), Loughborough, UK, 12–13 November 2012; pp. 1–4.
31. Yang, K.; Ekman, T.; Røste, T.; Bekkadal, F. A quasi-deterministic path loss propagation model for the open sea environment. In Proceedings of the 2011 The 14th International Symposium on Wireless Personal Multimedia Communications (WPMC), Brest, France, 3–7 October 2011; pp. 1–5.
32. Yang, K.; Molisch, A.F.; Ekman, T.; Røste, T.; Berbineau, M. A round earth loss model and small-scale channel properties for open-sea radio propagation. *IEEE Trans. Veh. Technol.* **2019**, *68*, 8449–8460. [CrossRef]
33. Yang, K.; Molisch, A.F.; Ekman, T.; Røste, T.; A deterministic round earth loss model for open-sea radio propagation. In Proceedings of the 2013 IEEE 77th Vehicular Technology Conference (VTC Spring), Dresden, Germany, 2–3 June 2013; pp. 1–5.
34. Shannon. Shannon-Hartley Theorem. Available online: https://en.wikipedia.org/wiki/Shannon%E2%80%93Hartley_theorem (accessed on 1 July 2021).